RSC Advances

PAPER

View Article Online
View Journal | View Issue

Cite this: *RSC Adv.*, 2024, **14**, 9391

Sesquiterpenoids and hexanorcucurbitacin from *Aquilaria malaccensis* agarwood with anti-inflammatory effects by inhibiting the STAT1/AKT/MAPK/NLRP3 pathway†

Chi Thanh Ma, ‡[ab] Tianqi Huang,‡[bc] Jae Sik Yu, ‡[b] Tu Loan Ly, [d] Kim Long Vu Huynh,[d] Sung Won Kwon, [e] Jeong Hill Park [e] and Hyun Ok Yang *[b]

Received 20th December 2023
Accepted 11th March 2024

DOI: 10.1039/d3ra08686k

rsc.li/rsc-advances

Seven unknown compounds **1–7**, including four sesquiterpenoids, one azulene-type, one indene-type, and one rare hexanorcucurbitacin, together with eleven knowns ones (**8–16**), were isolated from the agarwood chips of *Aquilaria malaccensis*. The structures of the isolated compounds were elucidated by extensive spectroscopic methods such as mass spectrometry, UV, IR, NMR spectroscopy. The precise stereochemical configurations of new compounds were determined by calculated ECD spectra data, as well as a single-crystal X-ray diffraction analysis. The isolated compounds **1–7** were evaluated by estimating the levels of nitric oxide (NO), TNF-α, and the expression of enzyme iNOS, and COX-2. Among them, a rare hexanortriterpenoid (**7**) derived from a cucurbitane-type triterpenoid showed the significantly attenuated neuro-inflammatory effects *via* the STAT1/AKT/MAPK/NLRP3 signaling pathway on the mechanistic studies.

Introduction

Inflammation has become a major global health issue in recent years.[1] Although inflammation is a normal physiological body response against a toxic stimulus to maintain body homeostasis.[2] Emerging evidence has demonstrated that neuroinflammation plays a causal role in the pathogenesis of neurodegenerative diseases in the central nervous system (CNS), including Alzheimer's disease (AD) and Parkinson's disease.[3] Pro-inflammatory cytokines production is associated with an increase of Aβ concentration in AD mice models, suggesting Aβ to be a key factor that drives neuroinflammation.[4] As the resident phagocytes and innate immune cells of the CNS, microglia are vital in the progression of neurodegenerative diseases by mediating neuroinflammatory responses.[5] Nevertheless, when subjected to prolonged activation, microglia undergo functional alterations, notably an excessive production of pro-inflammatory cytokines. Therefore, targeting microglia-mediated neuroinflammation may be an effective therapy to protect neurons in neurodegenerative disease.

Natural compounds derived from plant species have been proven to have various biological functions, including immune regulation, antitumor, and other health benefits with low toxicity.[6] Many types of phytochemicals can regulate inflammation in CNS by regulating oxidative stress, and signal transduction of inflammatory pathways.[7] Therefore, they have long been widely used in the medical field, the catering industry, and other areas of human life. The pathogenesis of neurodegenerative disease is associated with immune disorders and inflammation, oxidative stress,[8] which indicates that plant compounds may potentially be developed as a therapeutant.

A. malaccensis, known as agarwood, belongs to the Thymelaeaceae family, which is widely spread in South Asia. *A. malaccensis* is used in traditional herbal medicine to relieve epilepsy, rheumatism, inflammation, weakness, bronchitis, and in the treatment of snake bites.[9] And recently, *in vivo* and *in vitro* studies reported the phytomedicinal uses of agarwood of anti-inflammatory, immunomodulatory, anti-obesity, antidiabetic activity in asthma, neurological disorders, stress and anxiety

[a]*Faculty of Pharmacy, University of Medicine and Pharmacy at Ho Chi Minh City, 41-43 Dinh Tien Hoang St, Dist 1, Ho Chi Minh City 700000, Vietnam. E-mail: mcthanh@ump.edu.vn*

[b]*Department of Integrative Biological Sciences and Industry & Convergence Research Center for Natural Products, Sejong University, 209, Neungdong-ro, Gwangjin-gu, Seoul 05006, Republic of Korea. E-mail: jsyu@sejong.ac.kr; hoyang@sejong.ac.kr; Fax: +82-02-3408-4336; Tel: +82-02-3408-1959*

[c]*Korea Institute of Science and Technology (KIST) School, Korea University of Science and Technology (UST), 5 Hwarang-ro 14-gil, Wolgok 2(i)-dong, Seongbuk-gu, Seoul 02792, Republic of Korea. E-mail: 618509@kist.re.kr*

[d]*Faculty of Pharmacy, Ton Duc Thang University, Ho Chi Minh City, Vietnam. E-mail: lytuloan@tdtu.edu.vn; vuhuynhkimlong@tdtu.edu.vn*

[e]*Research Institute of Pharmaceutical Sciences, College of Pharmacy, Seoul National University, 1 Gwanak-ro, Gwanak-gu, Seoul 08826, Republic of Korea. E-mail: swkwon@snu.ac.kr; hillpark@snu.ac.kr*

† Electronic supplementary information (ESI) available: Detailed experimental procedure, 1D and 2D NMR, IR, $[\alpha]_D^{20}$, UV, ECD, MS spectra data of **1–7** are included herein. X-ray crystallography data for **7** (CIF). CCDC 2033830. For ESI and crystallographic data in CIF or other electronic format see DOI: **https://doi.org/10.1039/d3ra08686k**

‡ These authors contributed equally.

reduction, cancer, and others.[10] While *A. malaccensis* and agarwood have shown potential in various areas of traditional medicine, scientific research is still ongoing to validate these claims and to better understand the specific bioactive compounds responsible for these effects.

Hence, this study demonstrates the phytochemical investigation of the extract of *A. malaccensis* and the pharmacological activities of seven previously undescribed compounds. The isolated novel compounds were investigated for their potential to attenuate NO production and signalling from LPS-stimulated BV-2 cell in the present study.

Results and discussion

Compound **1** was obtained as a colorless oil with specific optical rotation $[\alpha]_D^{20}$ −81.2 (*c* 0.1, MeOH). The HRESI-MS spectrum of **1** showed a positive ion peak at *m/z* 249.1479 $[M + H]^+$ (calcd for $C_{15}H_{21}O_3$, 249.1485), corresponding to the molecular formula $C_{15}H_{20}O_3$, implying 5 degrees of unsaturation. The measured CD spectrum of **1** exhibited a negative cotton effect around 220 nm due to the n → π* transition of the ketone group. The ^{1}H NMR data (Table 1) revealed the presence of one olefinic (δ_H 5.82 dd, J = 4.0, 1.6 Hz, H-2), one oxymethine (δ_H 4.22, dd, J = 12.0, 1.6 Hz, H-8), three aliphatic methines (δ_H 2.58 (H-11), 2.56 (H-5), and 2.39 (H-4)), and three methyl groups (δ_H 1.32 (H_3-14), 1.12 (H_3-13), and 1.05 (H_3-15)). The ^{13}C NMR data (Table 2) showed the presence of 15 carbon signals, including one carbonyl group at δ_C 181.7 (C-12), three nonprotonated carbons at δ_C 158.6 (C-1), 79.8 (C-1), and 73.4 (C-1), five methine carbons at δ_C 127.7 (C-2), 84.6 (C-8), 50.1 (C-11), 44.5 (C-5) and 41.8 (C-4), three methylene carbons at δ_C 40.2 (C-9), 39.1 (C-3), and 36.7 (C-6), and three methyls at δ_C 33.1 (C-14), 16.4 (C-15), and 8.23 (C-13). These data suggest that **1** is a guaiane-type sesquiterpene lactone. The ^{1}H–^{1}H COSY spectrum revealed the correlations of two spin-coupling systems of H-2/H_2-3/H-4(/H_3-15)/H-5/H_2-6 and H-8/H_2-9 (Fig. 2). The key HMBC correlations were observed

Table 1 ^{1}H NMR spectroscopic data of **1–6** in CD_3OD and $CDCl_3$

	1 (CD_3OD)[c]	**2** (CD_3OD)[a]	**3** ($CDCl_3$)[c]	**4** ($CDCl_3$)[b]	**5** ($CDCl_3$)[c]	**6** ($CDCl_3$)[c]
No.	δ_H mult (*J*, Hz)	δ_H mult (*J*, Hz)	δ_H mult (*J*, Hz)	δ_H mult (*J*, Hz)	δ_H mult (*J*, Hz)	δ_H mult (*J*, Hz)
1a	—	—	—	2.24 m	—	
1b	—	—	—	2.30 ddd (14.5, 5.5, 2.0)	—	
2a	5.82 dd (4.0, 1.6)	—	4.00 dd (9.6, 6.4)	1.85 dddd (12.0, 8.0, 5.5, 3.0)	1.97 m	1.97 m
2b	—	—		1.42 m	1.93 m	
3a	2.23 ddd (16.0, 7.2, 3.2)	2.70 dd (18.8, 6.4)	1.96 ddd (13.6, 8.8, 7.2)	1.43 m	1.91 m	2.05 m
3b	1.98 ddt (16.0, 10.4, 1.6)	1.98 dd (18.8, 1.2)	1.80 ddd (13.6, 9.6, 6.4)	1.54 ddd (12.0, 8.0, 5.0)	1.24 m	1.47 m
4	2.39 m	2.79 m	2.57 m	1.42 m	2.72 m	2.71 m
5	2.56 m	—	1.87 m		1.78 ddd (11.2, 5.6, 1.6)	2.29 dt (12.8, 6.4)
6a	1.90 dd (13.6, 3.2)	2.59 d 14.4	1.85 dd (20.0, 10.4)	1.99 dd (13.0, 4.5)	1.75 dtd (14.4, 4.0, 1.6)	2.09 dd (16.0, 12.8)
6b	1.27 t (12.8)	—	1.53 dd (20.0, 9.6)	1.44 m	1.37 dddd (14.4, 12.8, 11.2, 5.6)	2.38 dd (16.0, 6.4)
7a	—	—	—		2.60 dt (18.4, 4.0)	
7b	—	—			2.46 ddd (18.4, 12.8, 4.0)	
8	4.22 dd (12.0, 1.6)	—	3.48 overlap			5.74 s
9a	2.57 dd (14.4, 11.2)	—	1.74 m	5.68 d (2.0)	5.74 s	
9b	1.88 dd (14.4, 1.6)	—	1.68 m			
10a	—	—	2.10 td (13.6, 4.0)			2.00 d (1.0)
10b			1.56 m			
11a	2.58 q (7.2)	2.48 dd (11.6, 1.2)		2.50 dd (15.0 4.5)	1.99 s	0.93 d (7.2)
11b	—	2.03 d (11.6)				
12a	—	—	4.71 d (1.6)	1.20 d (2.5)	1.00 d (7.2)	
12b			4.73 d (1.6)			
13	1.12 d (6.4)	1.04 s	1.69 s			
14	1.32 s	1.38 s	1.18 s			
15a	1.05 d (7.2)	1.06 d (7.2)	3.96 dd (10.4, 1.6)			
15b			3.62 dd (10.4, 1.6)			
13-OCH_3		3.68 s				

[a] Data were measured at 400 MHz (^{1}H) and 100 MHz (^{13}C). [b] Data were measured at 500 MHz (^{1}H) and 125 MHz (^{13}C). [c] Data were measured at 800 MHz (^{1}H) and 200 MHz (^{13}C).

Table 2 ^{13}C NMR spectroscopic data of **1–6** in CD_3OD and $CDCl_3$

	1 (CD_3OD)[c]	**2** (CD_3OD)[a]	**3** ($CDCl_3$)[c]	**4** ($CDCl_3$)[b]	**5** ($CDCl_3$)[c]	**6** ($CDCl_3$)[c]
No.	δ_C	δ_C	δ_C	δ_C	δ_C	δ_C
1	158.6	143.3	46.4	32.9	86.4	82.5
2	127.7	206.8	82.5	26.2	37.0	36.8
3	39.1	44.7	38.9	30.3	29.3	30.4
4	41.8	34.3	51.7	43.6	35.8	34.7
5	44.5	178.1	38.8	39.6	55.9	52.9
6	36.7	39.9	35.9	38.6	18.3	36.7
7	79.8	77.6	73.4	72.5	42.9	198.7
8	84.6	217.1	75.3	203.5	203.6	125.4
9	40.2	64.7	30.1	124.6	126.2	164.1
10	73.4	42.5	33.8	172.0	155.5	19.1
11	50.1	45.9	146.1	51.2	22.6	14.9
12	181.7	171.1	110.3	24.6	15.8	
13	8.23	14.9	19.9	28.3		
14	33.1	16.0	28.1	15.2		
15	16.4	17.9	67.4	15.9		

[a] Data were measured at 100 MHz (^{13}C). [b] Data were measured at 125 MHz (^{13}C). [c] Data were measured at 200 MHz (^{13}C).

from H-2 to C-1/C-3/C-4/C-5/C-10, from H_2-3 to C-1/C-2/C-4/C-5/C-15, from H-4 to C-3/C-5/C-6/C-15, from H_2-6 to C-1/C-4/C-5/C-7/C-8/C-11, from H-8 to C-7/C-9/C-10, from H_2-9 to C-1/C-7/C-8/C-10, from H-11 to C-6/C-7/C-8/C-12/C-13, from H_3-13 to C-7/C-11/C-12, from H_3-14 to C-1/C-9/C-10, and from H_3-15 to C-3/C-4/C-5 (Fig. 2). The NOESY correlations were observed between H-4 and H-3a/H-5, between H-6a and H-5/H_3-13, between H-9a and H_3-14 suggest that H-3a, H-4, H-5, H-6a, H-9a, H_3-13, and H_3-14 were in α-orientation. Correlations between H-8 and H-6b/H-9b/H-11, between H_3-15 and H-3b in the NOESY spectrum, indicated that H-8, H-11, and H_3-15 were in the β-orientation (Fig. S6†). The absolute configuration of **1** was assigned as 4*S*,5*S*,7*S*,8*S*,10*S*,11*R* by the comparison of calculated and experimental ECD spectra, as shown in Fig. 3. Therefore, the structure of **1** was elucidated as 7α,10β-dihydroxy-4αH,5αH,8βH,11βH-guaia-1(2)-en-12,8α-olide.

Table 3 ^{1}H (800 MHz) and ^{13}C (200 MHz) NMR spectroscopic data of **7** in $CDCl_3$

	7	
No.	δ_C	δ_H mult (*J* in Hz)
1	115.4	6.11 d (2.4)
2	144.5	—
3	198.7	—
4	47.5	—
5	136.5	—
6	120.2	5.73 dt (4.8, 2.4)
7	23.4	2.44 ddt (19.6, 8.8, 2.4) 2.03 ddd (19.6, 5.2, 2.4)
8	40.6	2.29 m
9	49.0	—
10	35.3	3.44 p (2.4)
11	212.6	—
12	44.6	3.16 d (15.2) 3.02 d (15.2)
13	49.8	—
14	52.2	—
15	42.8	2.30 dt (16.8, 2.4) 2.20 dd (16.8, 4.0)
16	143.7	6.68 dd (4.0, 2.4)
17	151.2	—
18	22.8	0.96 s
19	20.9	1.09 s
20	196.2	—
21	26.9	2.28 s
28	27.5	1.19 s
29	20.2	1.32 s
30	19.0	1.16 s
2-OH		5.84 s

Compound **2** was isolated as colorless oil with specific optical rotation $[\alpha]_D^{20}$ −98.0 (*c* 0.1, MeOH). Its molecular formula was $C_{15}H_{24}O_2$ based on the HRESI-TOF/MS ion peak at *m*/*z* 293.1380 $[M + H]^+$ (calcd for $C_{16}H_{20}O_5$, 293.1384), indicating seven degrees of unsaturation. The UV spectrum of **2** revealed the presence of conjugated carbonyl chromophores of absorption maxima at λ_{max} 240 nm. The measured CD spectrum of **2** exhibited a negative cotton effect around 230 nm due to the n → π* transition of the ketone group. The ^{1}H NMR spectrum of **2** showed the signals of one methine at δ_H 2.79 (H-4), three methylenes, three methyls [δ_H 1.38 (s, CH_3-14), 1.06 (d, $J = 7.2$, CH_3-15), and 1.04 (s, CH_3-13)], and one methoxy at δ_H 3.68 (12-OCH_3). The ^{13}C NMR spectrum of **2** revealed the presence of 16 carbon signals, including two ketone groups at δ_C 217.1 (C-8) and 206.8 (C-2), one carbonyl (δ_C 171.1, C-12), one aliphatic methine carbon (δ_C 34.3 (C-4)), five non-protonated carbons (δ_C 178.1 (C-5), 143.3 (C-1), 77.6 (C-7), 64.7 (C-9), and 42.5 (C-10)), three methylene carbons (δ_C 45.9 (C-11), 44.7 (C-3), and 39.9 (C-6)), three methyls (δ_C 17.9, 16.0 and 14.9), and one methoxy group (δ_C 51.4). The afore-mentioned data suggested that **2** was a guaiane-type sesquiterpenoid. The ^{1}H–^{1}H COSY revealed the correlations of consecutive aliphatic protons of H_2-3/H-4/H_3-15 (Fig. 2). The key HMBC correlations were observed from H_2-2 (δ_H 2.70, dd, $J = 18.8$, 6.4 Hz and 1.37, dd, $J = 18.8$, 1.2 Hz) to C-

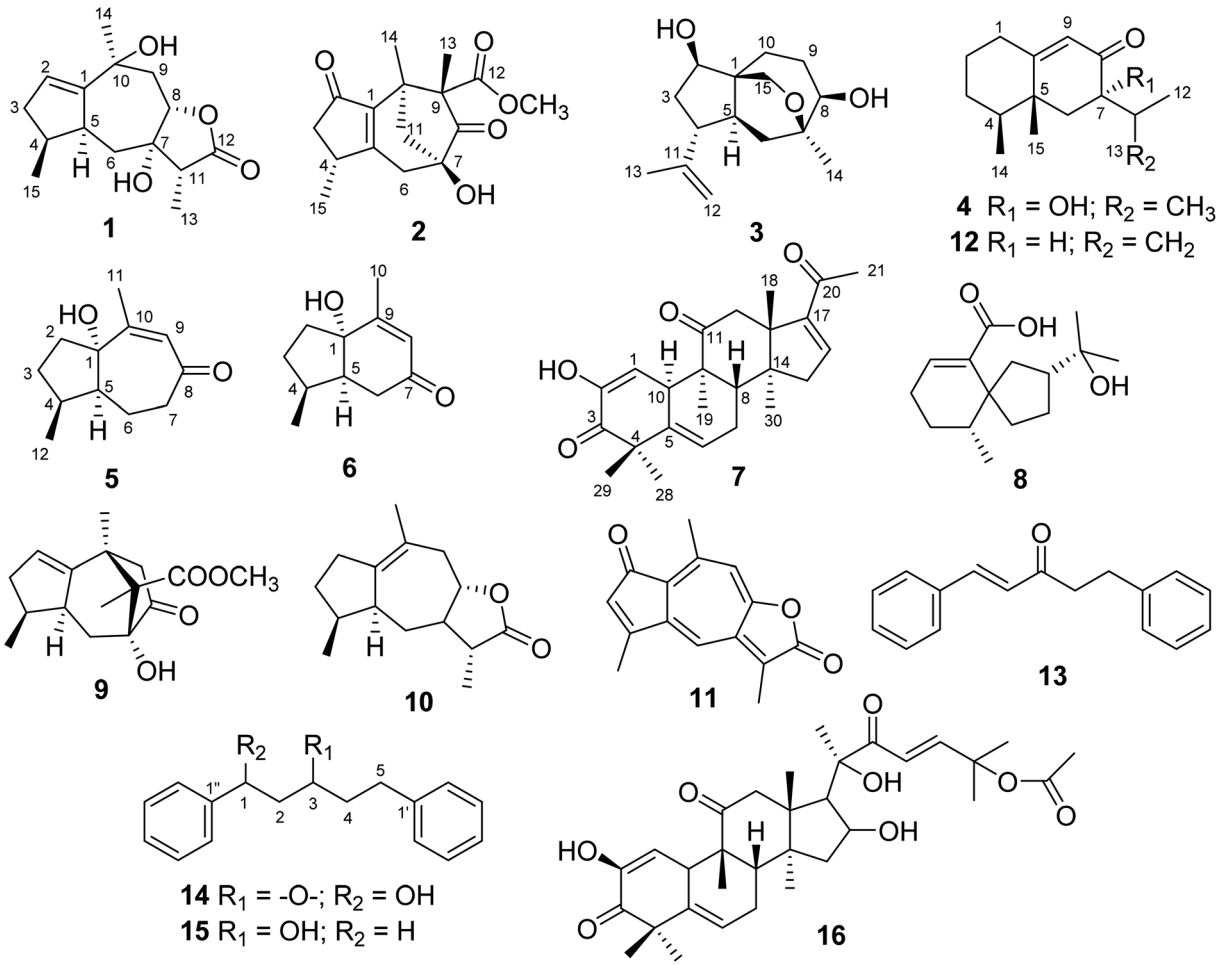

Fig. 1 Chemical structure of compounds 1–16.

2/C-4/C-5/C-15, from H-4 and C-3/C-5/C-15, from H_2-6 (δ_H 2.59, d, J = 14.4 Hz) to C-1/C-5/C-7/C-8/C-11, from H_2-11 (δ_H 2.48, dd, J = 11.6, 1.2 Hz and 2.03, d, J = 11.6 Hz) to C-1/C-6/C-7/C-8/C-9/C-10/C-14, from H_3-15 to C-3/C-4/C-5 (Fig. 2). In addition, the HMBC cross-peaks of CH_3-13 with C-8, C-9, C-10, and C-12, and of H_3-14 with C-1, C-9, C-10, and C-11, which exhibited the

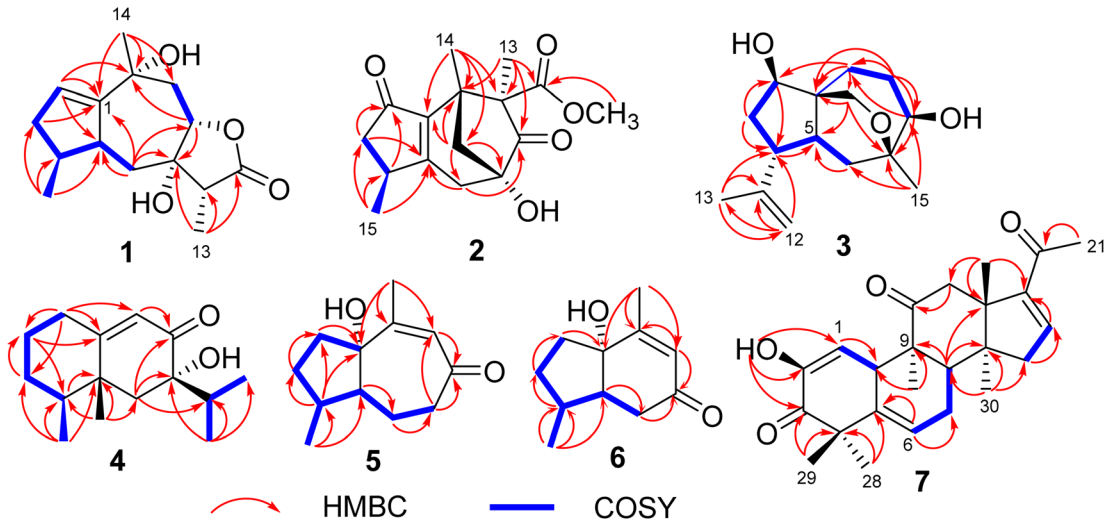

Fig. 2 Key HMBC, ^{1}H–^{1}H COSY correlations of 1–7.

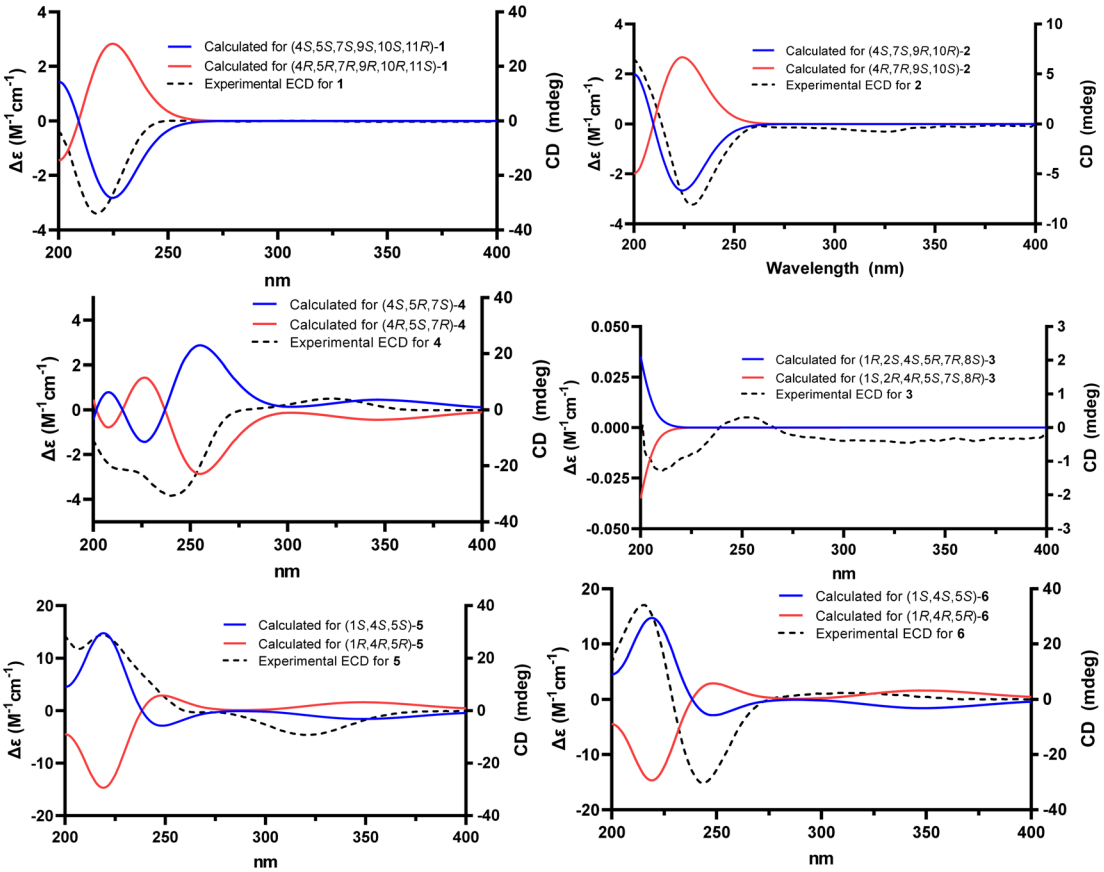

Fig. 3 Experimental and calculated ECD spectra of **1**–**6**.

linkage of the carbon bridge between C-7 and C-10 and methylene group of CH_2-11 on the bridge (Fig. 2). The ^{13}C NMR and ^{1}H NMR data of **2** were similar to those of chamaejasmone C[11] except that the number of ^{13}C NMR signals of **3** was 16 in total, while chamaejasmone C showed 15 ^{13}C signals. The main difference was that the methylene group at C-12 in chamaejasmone C changed to the acetyl group (δ_C 171.1, C-12) in **3.** The relative configuration of **2** was assigned from the NOESY spectrum. The NOESY correlations between H_3-15 and H-3b, H_2-6, between H_2-11 and H_2-6, H_3-14, suggested that these protons are the same β-orientation. The absolute configuration of **2** was assigned as 4*R*,7*R*,9*S*,10*S* by the comparison of calculated and experimental ECD spectra, as shown in Fig. 3. Thus, the structure of **2** was determined and named as chamaejasmone G.

Compound **3** win obtained as colorless oil with specific optical rotation $[\alpha]_D^{20}$ −73.0 (*c* 0.1, MeOH). Its positive HRESI-TOFMS spectral data exhibited the pseudomolecular ion peak at *m*/*z* 253.1790 $[M + H]^+$, consistent with the molecular formula of $C_{15}H_{24}O_3$ (calcd for $C_{15}H_{25}O_3$, 237.1798), indicating four degrees of unsaturation. The ^{1}H NMR spectrum of **3** showed six methylenes (including one oxymethylene and one terminal methylene), four methines, and two methyls (δ_H 1.69 s, H_3-13 and 1.18 s, H_3-14). The ^{13}C NMR spectrum of **3** exhibited the presence of 15 carbon signals, including one olefinic carbon (δ_C 110.3, C-12), three non-protonated carbons (δ_C 146.1 (C-11), 73.4 (C-7), and 46.4 (C-1)), four aliphatic methine carbons (δ_C 82.5 (C-2), 75.3 (C-8), 51.7 (C-4), and 38.8 (C-5)), five methylene carbons (δ_C 67.4 (C-15), 38.9 (C-3), 35.9 (C-6), 33.8 (C-10), and 30.1 (C-9)), and two methyl groups (δ_C 28.1 (C-14) and 19.9 (C-13)). These data suggested that compound **3** was an isodaucane-type sesquiterpenoid. The ^{1}H–^{1}H COSY spectrum revealed the correlations of two-spin systems of H-2/H_2-3/H-4/H-5/H_2-6 and H-8/H_2-9/H_2-10. The key HMBC spectrum exhibited the correlations from H_2-9 (δ_H 1.74 and 1.68) to C-1/C-7/C-8/C-10, from H_2-10 (δ_H 2.10 and 1.56) to C-1/C-2/C-5/C-8/C-9/C-15, from H-2 (δ_H 4.00, dd, J = 9.6, 6.4 Hz) to C-4/C-10/C-15, from H_2-3 (δ_H 1.96, ddd, J = 13.6, 8.8, 7.2 Hz and 1.80, ddd, J = 13.6, 9.6, 6.4 Hz) to C-1/C-2/C-4/C-5/C-11, from H-4 (δ_H 2.57) to C-3/C-5/C-6/C-12/C-13, from H_2-6 (δ_H 1.85 and 1.53) to C-4/C-5/C-7/C-8/C-14, from H_2-12 to C-4/C-11/C-13, from H_3-13 to C-4/C-11/C-12, H_3-14 to C-6/C-7/C-8 (Fig. 2). Furthermore, correlations were observed from H_2-15 to C-1/C-5/C-7/C-10, which established the carbon bridge between C-1 to C-7 *via* oxymethylene C-15. The relative configuration of **3** was assigned from NOESY correlations. The cross-peak correlations were observed between H-4 and H-3a/H-3b/H-6b/H-11a/H_2-12, between H-15a and H-3b/H-4/H-6b, suggested that these protons were on the same site β-orientation. The NOESY spectrum showed the correlations between H-2 and H-3a/H-6a/H-10b, indicated that these protons were on α-orientation. The absolute configuration of **3** were confirmed by comparison of the experimental and calculated ECD spectra data. The experimental ECD curve of **3** was identical with the

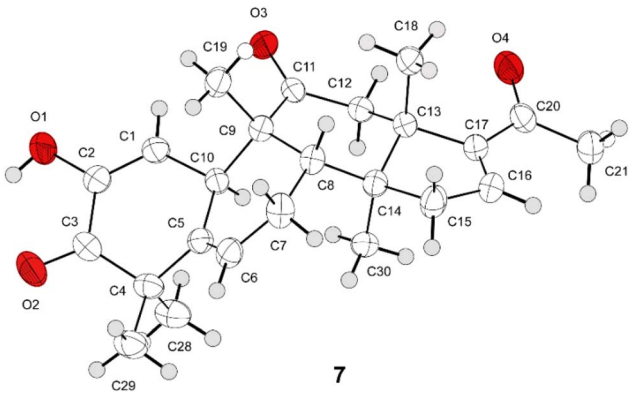

Fig. 4 X-ray crystallographic structure of **7**.

calculated for (1*S*,2*R*,4*R*,5*S*,7*S*,8*R*) as shown in Fig. 3. Hence, compound **3** was identified and named as isodaucanranol A.

Compound **4** was isolated as colorless oil with specific optical rotation $[\alpha]_D^{20}$ −69.0 (*c* 0.07, MeOH). Its molecular formula was $C_{15}H_{24}O_2$ based on the HRESI-TOF/MS ion peak at *m*/*z* 237.1839 $[M + H]^+$ (calcd for $C_{15}H_{25}O_2$, 237.1855), indicating four degrees of unsaturation. The ^{1}H NMR data of **4** displayed signal resonances for an olefinic proton (δ_H 5.68, d, $J = 2.0$, H-9) and four methyls (δ_H 1.20, 1.19, 1.11 and 0.91). The ^{13}C NMR spectrum (Table 2) revealed 15 carbon signals, including four methyls (δ_C 28.3 (C-13), 24.6 (C-12), 15.9 (C-8), and 15.2 (C-14)), four methylenes (δ_C 38.6 (C-6), 32.9 (C-1), 30.3 (C-3), and 26.2 (C-2)), three methines (one olefinic), and three non-protonated carbons (one oxygenated, one olefinic), and a ketone group (δ_C 203.5, C-8). The 1D NMR spectroscopic data closely resembled to those of neopetasane (**12**),[12] an eremophilane sesquiterpene isolated from this plant. The main difference was that the terminal methylene in neopetasane was replaced by the methyl group in **4** and the presence of a hydroxyl group linked to C-7 in **4**. The structure of **4** was elucidated by the HMBC correlations from H_2-1 to C-2/C-3/C-9/C-10, H-6 to C-5/C-7/C-8/C-11/C-15; H-9 to C-1/C-5/, H-11 to C-6/C-7/C-8/C-12/C-13, H_3-15 to C-4/C-5/C-6/C-10 as depicted in Fig. 2. In the NOESY spectrum, the correlations between H-11/H_3-15/H_3-14 revealed that these protons were on β-orientation, whereas H-4 and 7-OH were on the opposite site α-orientation. The absolute

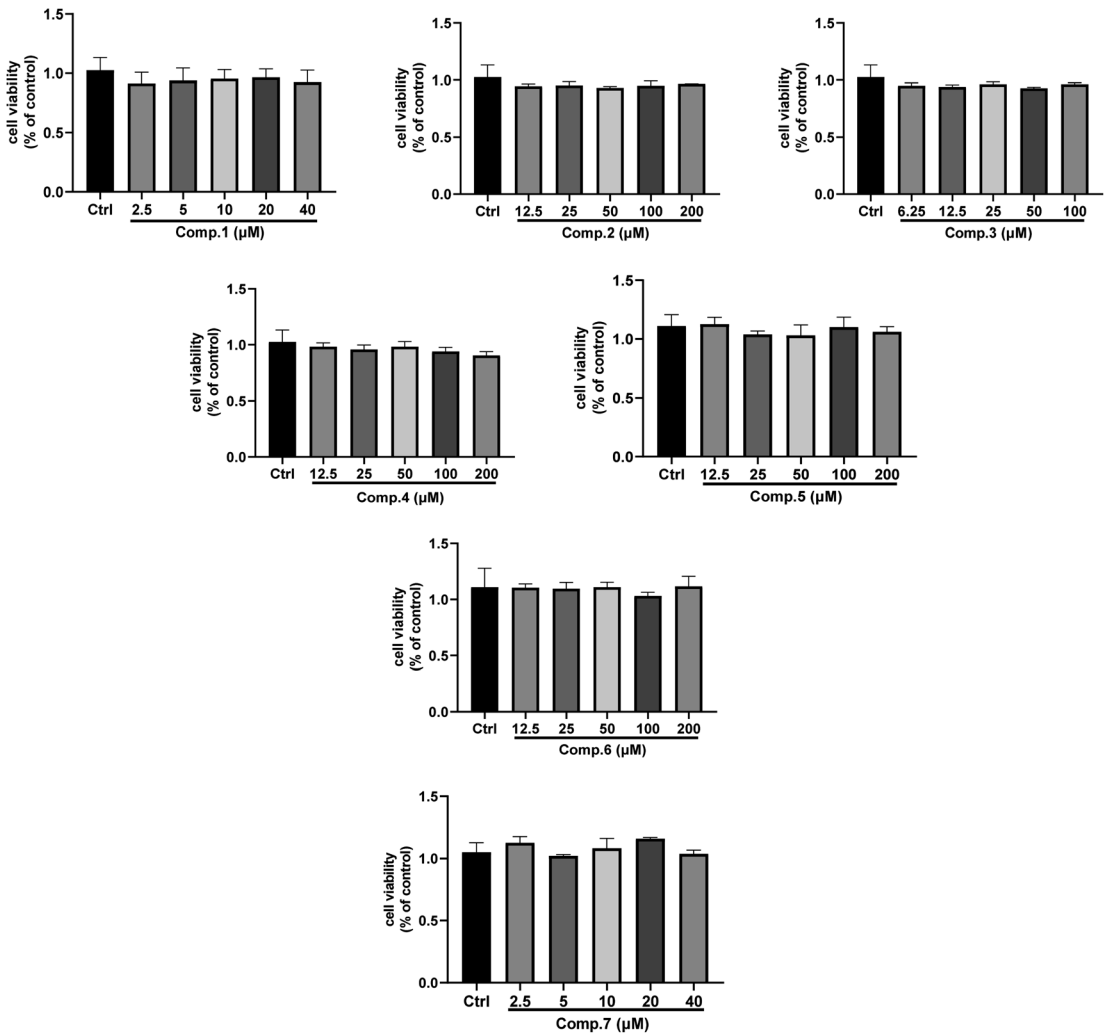

Fig. 5 Cell viability of compounds **1**–**7**.

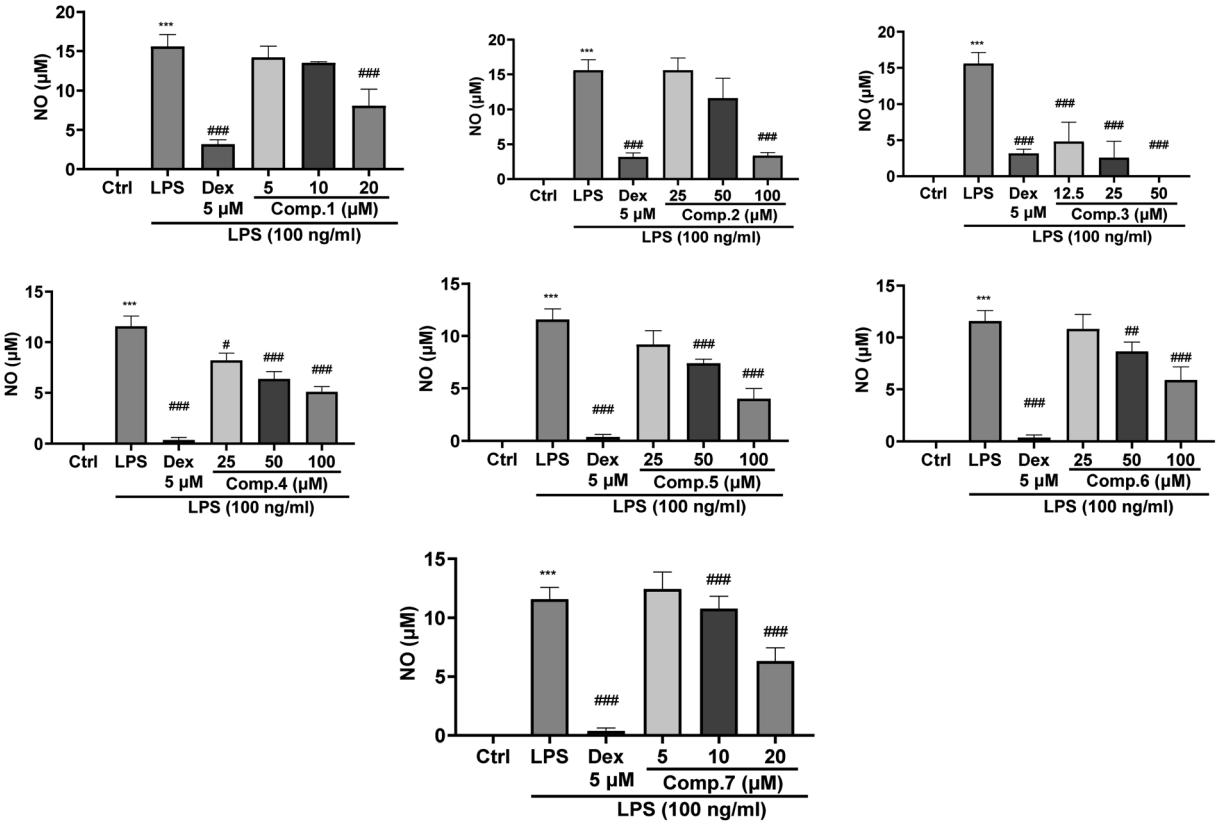

Fig. 6 NO production against LPS-induced microglial BV-2 cells of compounds **1**–**7**.

configuration of **4** was confirmed to be (4*S*,5*R*,7*S*) by comparison of ECD calculated values to experimental data (Fig. 3). Therefore, compound **4** was assigned as 7α-hydroxy-9(10)-ene-8-oxoeremophilane.

Compound **5** was obtained as a colorless oil. The molecular formula was elucidated from HRESI/TOF-MS as $C_{12}H_{18}O_2$ based on the ion peak at *m*/*z* 217.1180 $[M + Na]^+$ (calcd for $C_{12}H_{18}O_2Na$, 217.1204). The ^1H NMR spectrum (Table 1) displayed signals of an olefinic proton (δ_H 5.74, s), two methyl groups (δ_H 1.00 and 1.99). The ^{13}C NMR spectrum presented 12 carbon signals including three non-protonated carbons (one carbonyl and one oxygenated carbon), three methines (δ_C 126.2 (C-9), 55.9 (C-5), and 35.8 (C-4)), four methylenes (δ_C 42.9 (C-7), 37.0 (C-2), 29.3 (C-3), and 18.3 (C-6)), and two methyls. The spectroscopic data of **5** closely resembled to those of phaeocaulisin J,[13] a sesquiterpene isolated from *Curcuma phaeocaulis* and the difference from phaeocaulisin J was the absence of hydroxy group located at carbon C-4 in **5**. The planar structure of **5** was assigned by the HMBC correlations from H_3-12 to C-3/C-4/C-5, from CH_3-11 to C-1/C-9/C-10, from H_2-2 to C-1/C-3/C-4/C-5/C-9, from H-6 to C-1/C-4/C-5/C-7/C-8, and from H-9 to C-1/C-7/C-10/C-12 (Fig. 2). The relative configuration was solved by the NOESY correlations between H-4, H-5, and H_3-12. The key NOESY correlations were observed between H-4/H-5, H-5/H6b/H-7b, indicated that CH_3-12 was on β-orientation while H-4, H-5 were on α-orientation. The experimental ECD spectrum was highly consistent with the calculated for (1*S*,4*S*,5*S*) as shown in Fig. 3. Thus, the absolute configuration of **5** was

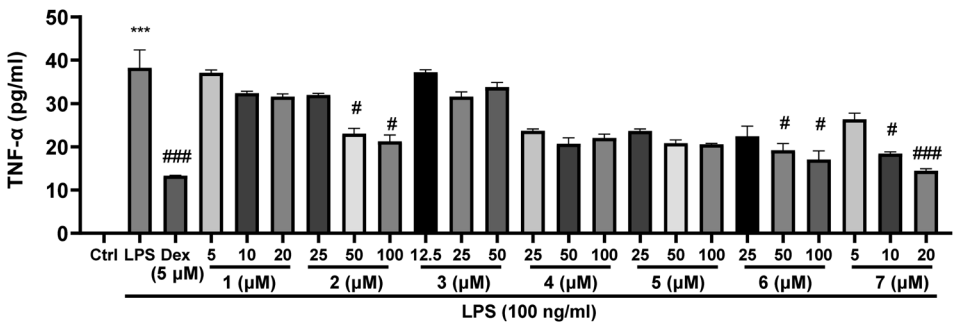

Fig. 7 TNF-α levels in the cells culture medium were determined using ELISA kit of compounds **1**–**7**. Data are detected as mean ± SEM ($n = 3$). ***: $P < 0.001$, the significant difference compared with the control. Compared with LPS group, #: $p < 0.05$, ###: $p < 0.001$.

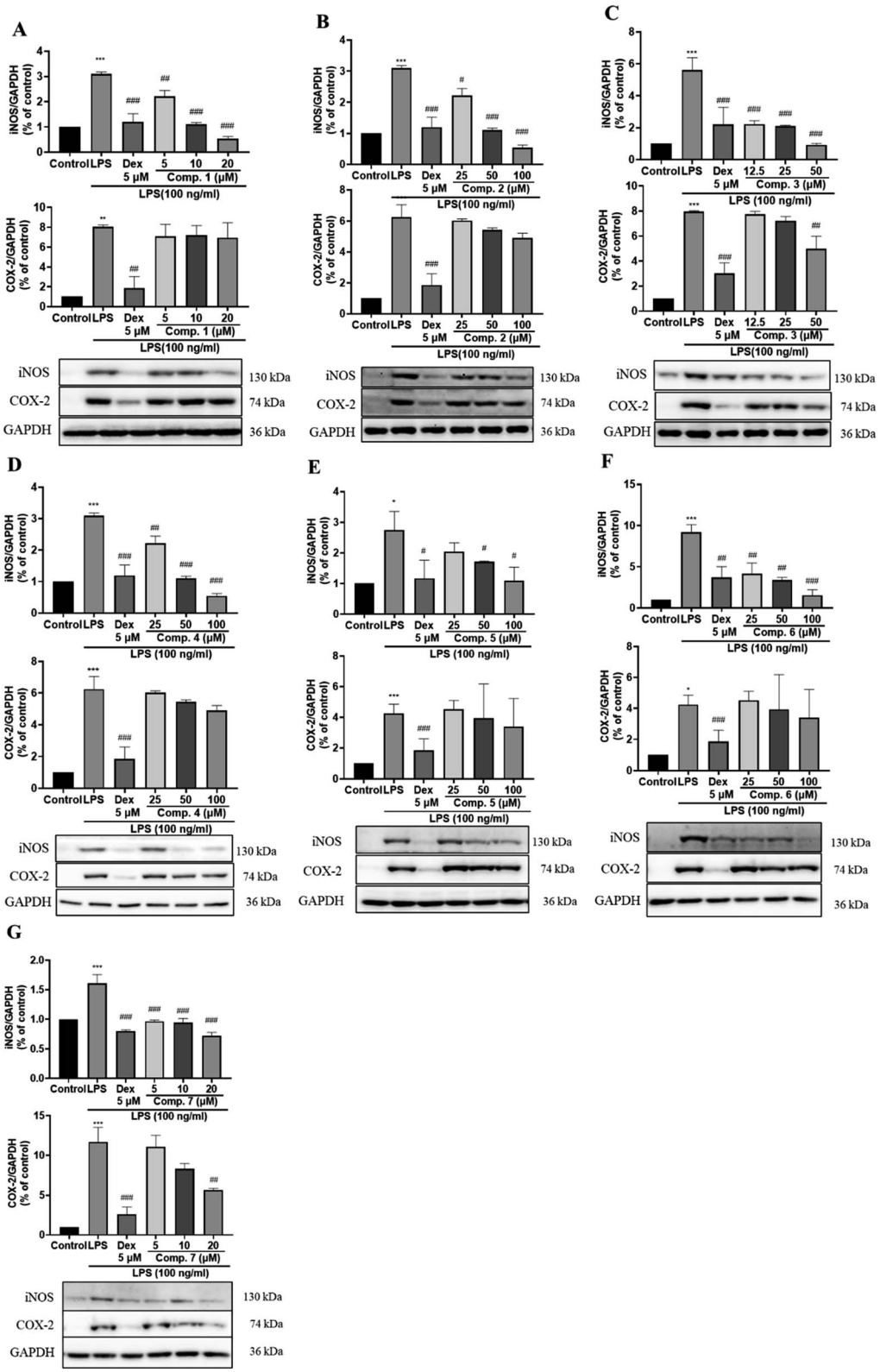

Fig. 8 The expression of inflammatory enzymes iNOS and COX-2 by compounds **1–7** (A–G) on LPS-activated microglial cells.

identified as (1*S*,4*S*,5*S*)-1-hydroxy-4,10-dimethyl-hexahydro-azulen-8-one.

Compound **6** was isolated as a colorless oil, of which molecular formula was determined as $C_{11}H_{16}O_2$ from the HRESI-TOF/MS by positive ion peak at *m*/*z* 181.1222 $[M + H]^+$, (calcd for $C_{11}H_{17}O_2$, 181.1229). The UV spectrum showed an absorption maximum at 235 nm, suggesting the presence of an α,β-unsaturated carbonyl moiety. The ^{1}H NMR data (Table 1) of

6 exhibited the signals of an olefinic proton (δ_H 5.74, s), two methyl groups (δ_H 0.93 and 2.00). The ^{13}C NMR (Table 2) and HSQC data of **6** showed 11 carbon signals including one ketone group (δ_C 198.7, C-7), one olefinic quaternary carbon (δ_C 164.1, C-9), one oxygenated carbon (δ_C 82.5, C-1), three methylenes (δ_C 36.8 (C-2), 36.7 (C-6), and 30.4 (C-3)), three methines (δ_C 125.4 (C-8), 52.9 (C-5) and 34.7, C-4), and two methyls (δ_C 19.1, C-10 and 14.9, C-11). The ^1H–^1H COSY spectrum revealed the existence of a spin coupling system of H_2-2/H_2-3/H-4/H-5/H_2-6. Correlations were observed from H_3-11 to C-3/C-4/C-5, H_3-10 to C-1/C-8/C-9, H_2-2 to C-1/C-3/C-4/C-5/C-9; H-5 to C-1/C-2/C-3/C-4/C-6/C-7, and H-8 to C-1/C-6/C-7/C-9/C-10 in HMBC spectrum (Fig. 2). The cross peaks were observed in the NOESY spectrum between H-4 and H-3b/H-5/CH_3-11, CH_3-11 and H-3a/H-4/H_2-6. The absence of correlations between CH_3-11 and H-5 suggested that H-3b, H-4 and H-5 are in α-orientation and that H-3a, CH_3-11 are in β-orientation. The absolute configuration was determined based on the experimental ECD spectrum compared with the calculated of two possible enantiomers (Fig. 3). According to the empirical rule for α,β-unsaturated cyclohexanones, the negative cotton effect was observed at 244 nm due to the n – π* transition of ketone group (Fig. 3). Hence, the absolute configuration of **6** was (1*S*,4*S*,5*S*). Therefore, the structure of **6** was identified as (1*S*,4*S*,5*S*)-1-hydroxy-4,9-dimethyl-hexahydro-5*H*-inden-5-one.

Compound **7** was isolated as a colorless needle, had a molecular formula of $C_{24}H_{30}O_4$ determined from the ESI-TOF/MS by positive ion peak at *m*/*z* 383.2204 $[M + H]^+$, with 10 degrees of unsaturation. Three olefinic protons, two aliphatic protons, and six methyl singlet signals were interpreted from ^1H NMR spectrum (Table 3). The ^{13}C NMR spectrum (Table 3) of **7** revealed the presence of 24 carbon resonances corresponding to three ketocarbonyl groups, one oxygen-bearing sp^2 carbons, and three olefinic carbons. The remaining 17 carbons accounted for two methines, three methylenes, six methyls, and four quaternary carbons based on the HSQC experiment. The ^1H and ^{13}C data of **7** was identical to those of hexanorcucurbitacin I, isolated from *Ecballium elaterium*.[14] The only difference from hexanorcucurbitacin I was the hydroxyl moiety at C-16 changed into a double bond $\Delta^{16,17}$ in **7**, which was supported by the addition of one degree of unsaturation. The planar structure of **7** was identified by the ^1H–^1H COSY and HMBC spectral data (Fig. 2). The absolute configuration of **7** was established as (8*S*,9*S*,10*R*,13*S*,14*S*) by single-crystal X-ray diffraction analysis (Fig. 4). The structure of **7** was characterized as a rare hexanortriterpenoid derived from a cucurbitane-type triterpenoid, was named as 2-hydroxy-22,23,24,25,26,27-hexanorcucurbit-1,5,16-triene-3,11,20-trione.

Nine known compounds were identified as baimuxinic acid (**8**),[15] stelleraterpenoid B (**9**),[16] dihydrocollumellarin (**10**),[17] 2-oxo-guaia-1(10),3,5,7(11),8-pentaen-12,8-olide (**11**),[18] neopetasane (**12**),[12] 1,5-diphenyl-1-penten-3-one (**13**),[19] 1-hydroxy-1,5-diphenylpentan-3-one (**14**),[20] 1,5-diphenyl-3-pentanol (**15**),[21] cucurbitacin E (**16**),[22] by comparison of physical and spectroscopic data to those of reported in literature (Fig. 1). To the known compounds, **9–11** and **14–15** were first reported in *Aquilaria* genus.

Evaluation the neuro-inflammatory activities

Seven previously undescribed compounds (**1–7**) were evaluated for their *in vitro* neuro-inflammatory effects against NO production in LPS-stimulated microglial BV-2 cells.

NO and TNF-α secretions in LPS-induced BV-2 microglia cell under the treatment of *A. malaccensis* compounds. The cell viability of the isolated *A. malaccensis* compounds was evaluated in BV-2 microglia cells. All tested compounds did not display cytotoxicity after 24 h at the two-fold of the tested concentrations (Fig. 5). Subsequently, the secretion of NO and TNF-α were assessed for their anti-inflammatory properties by detecting their inhibitive effects on LPS-induced BV-2 microglia cells. Results showed that compounds **3–7** exhibited significant suppressive activity on the production of NO with inhibition

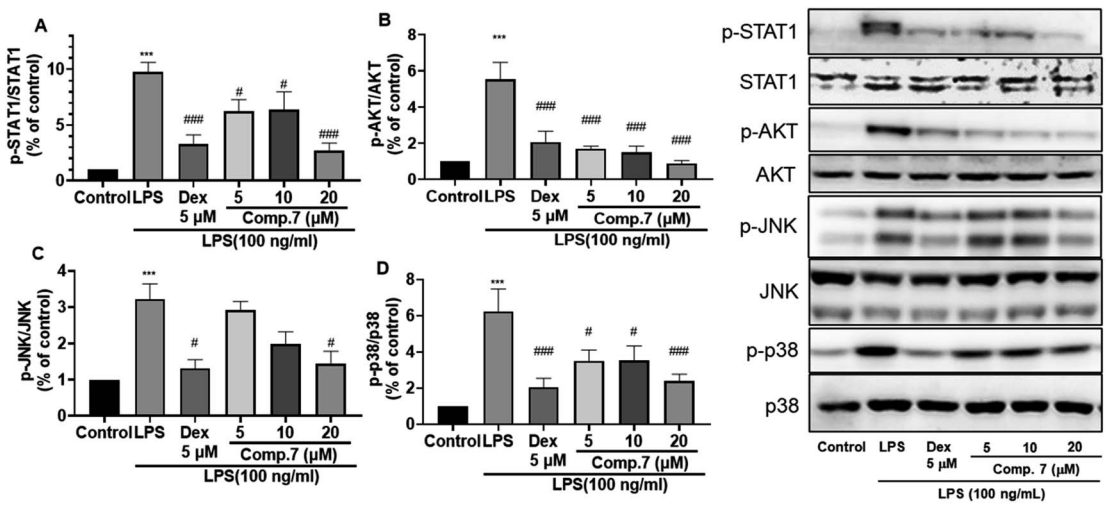

Fig. 9 The expression of STAT1/AKT/MAPK signaling by compound 7 on LPS-activated microglial cells. The phosphorylated level of STAT1 (A), AKT (B), JNK (C) and p38 MAPK (D) was detected. Dexamethasone (Dex) was positive control. Data are detected as mean (±SEM, $n = 4$). ***: $P < 0.001$, the significant difference compared with the control. Compared with LPS group, #: $p < 0.05$, ###: $p < 0.001$.

rate more than 50%, and compounds **1** and **2** showed mild potent inhibitory effect only under high concentration (100 μM and 20 μM, respectively) as depicted in Fig. 5, and for the TNF-α, only compounds **2**, **6**, and **7** showed good inhibition against LPS-induced TNF-α secretion (Fig. 7). Compounds **1** and **3** caused a mild increase in LPS-induced TNF-α secretion. Accordingly, compounds **2**, **6** and **7** exhibited the strongest activity, might be attributable to the anti-inflammation activity at *A. malaccensis* (Fig. 6).

Effects of *A. malaccensis* compounds on the expression of inflammatory enzymes in BV-2 microglial cells. The NO production is mainly mobilized by the upstream protein iNOS in the inflammatory signaling pathway. Inhibiting the NO release activation reveals reducing the activity of iNOS. To explore primary anti-inflammation mechanism, *A. malaccensis* compounds were performed to investigate the inhibitory effects on the iNOS enzymatic activation. As demonstrated in Fig. 7, the enzyme activity of iNOS simulated with LPS was significantly increased, while compounds **1**–**7** (Fig. 8A–G) strongly suppressed the iNOS enzymatic activation in a dose-dependent manner. Compounds **3** and **7** with the most significant effect in enzymatic activity by tested concentration were observed. Consist of the NO release, compound **5** (Fig. 8B) was found to be moderate effective in iNOS inhibition. The result revealed that compounds **1**–**7** significantly inhibited the production of NO by reducing the iNOS enzymatic activation.

LPS in microglia and epithelial cells induce COX-2, leading to its expression. In acute inflammation, COX-2 plays a role in the generation of TNF-α. The inhibition of the COX-2 activation of *A. malaccensis* compounds was performed in LPS-induced BV-

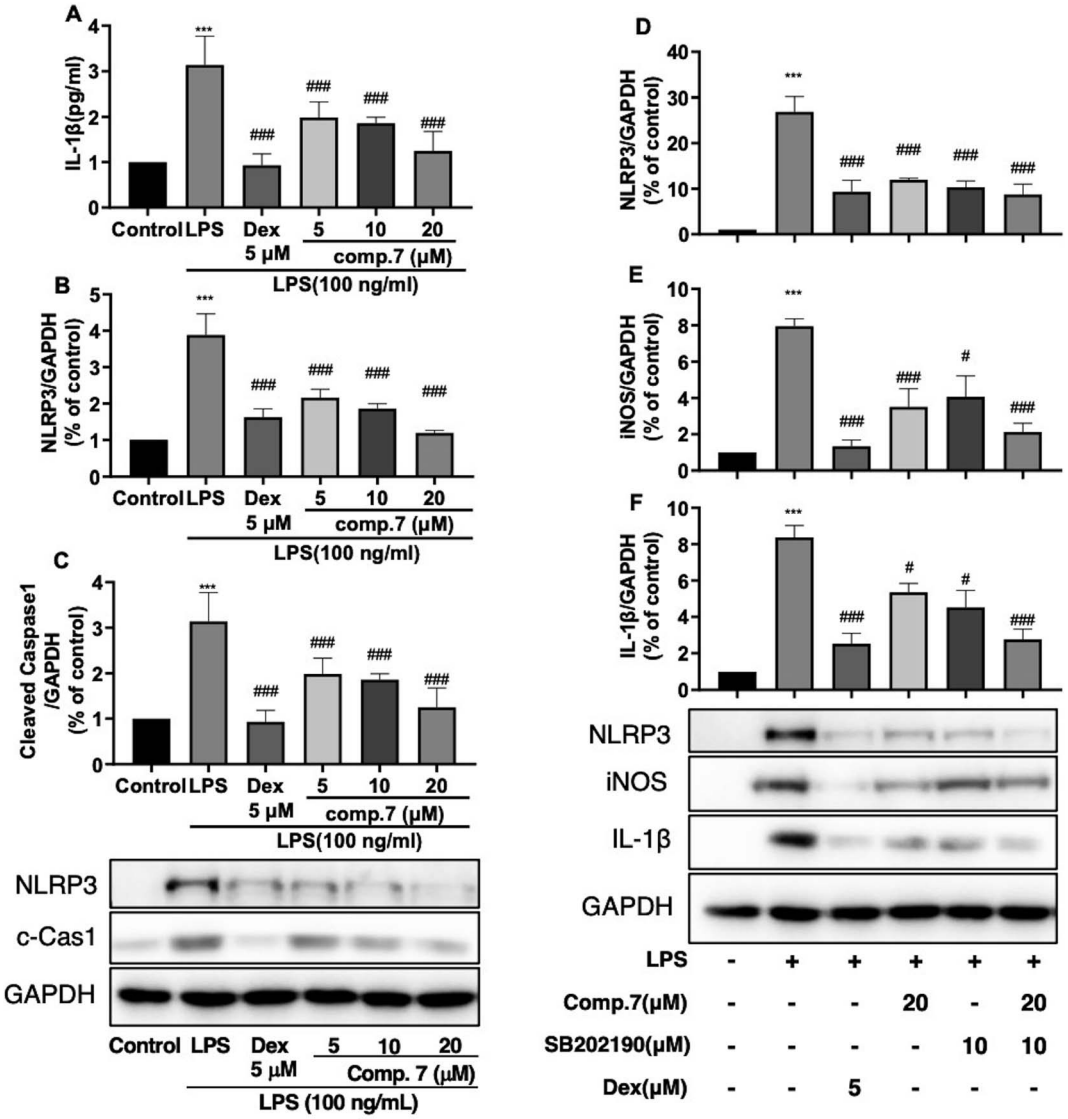

Fig. 10 The expression of MAPK/NLRP3 signaling and IL-1β production by compound **7** on LPS-activated microglial cells. The ELISA was performed to measure IL-1β (A) secretions as the manufacture protocol; respective western blots presenting the expression level of the NLRP3 (B), cleaved caspase1 (C), NLRP3 (D), iNOS (E) expression and IL-1β production (F) were detected after co-treatment with the specific inhibitor SB202190. Dexamethasone (Dex) was positive control. Data are detected as mean (±SEM, $n = 4$). ***: $P < 0.001$, the significant difference compared with the control. Compared with LPS group, #: $p < 0.05$, ###: $p < 0.001$.

2 microglia cells. In the present study, **3** and **7** were the most effective compounds by significantly reducing COX-2 expression (Fig. 8C and G). Whereas compounds **1–2** (Fig. 8A and B), and **4–6** (Fig. 8D–F) were not found to be effective in COX-2 inhibition.

Effects of *A. malaccensis* compound 7 on the expression of STAT1/AKT/MAPK signaling in BV-2 microglial cells. These results provide evidence that compound **7** exhibits the best anti-inflammatory activity on an *in vitro* model of CNS inflammation in *A. malaccensis* compounds. According to the results, compound **7** showed remarkable inhibitory effects on LPS-stimulated NO production, cytokine TNF-α, enzymatic iNOS, and COX-2 suppression. Thus, compound **7** was selected for further investigation on the mechanistic studies of neuro-inflammatory effects on LPS-induced BV-2 microglia cells.

The STAT1/AKT pathway participates in neuro-inflammatory responses.[23] To determine the effects of compound **7** on the LPS-activated STAT1/AKT/MAPK signaling pathway, BV2 cells were pre-treated with compound **7** for 1 h, followed by incubation with LPS for 24 h. LPS up-regulated the levels of p-STAT1, p-AKT, p-p38, p-JNK (Fig. 9), whereas the phosphorylation of these molecules was significantly suppressed by compound **7** during LPS stimulation. To the best of our knowledge, MAPK, PI3K/AKT, and STAT1 signaling are strongly integrated with microglia-induced neuroinflammation, which mainly stimulates inflammation *via* pro-inflammatory cytokines and marker release, apoptosis and oxidative stress.[24] Both the PI3K/AKT and MAPK pathways increase the nuclear translocation of the important transcription factor NF-κB, causing downstream NLRP3 inflammasome activation and assemble.[25] These results indicated that compound **7** regulated the LPS-induced neuro-inflammatory response by down-regulating the STAT1/AKT/MAPK pathway.

Effects of *A. malaccensis* compound 7 on the expression of MAPK/NLRP3 signaling in BV-2 microglial cells. NLRP3 inflammasome activation has been reported to be responsible for the release of IL-1β, which participates in the process of the inflammation and cytokine release *via* MAPK signaling.[26] Thus, we investigated whether compound **7** modulates the NLRP3 inflammasome. The results showed that compound **7** decreased the IL-1β pro-inflammatory cytokine levels, and the expression level of cleaved caspase1 also decreased (Fig. 10A–C). To further examine whether the NLRP3 inflammasome specifically regulated by MAPK in LPS-regulated microglial inflammation, the MAPK-specific inhibitor (SB202190) treated BV2 cells, to evaluate proinflammatory cytokine release and inflammation response activation treated with LPS for 24 h. The results showed that co-treatment of compound **7** and the MAPK inhibitor further decreased the IL-1β pro-inflammatory cytokine expression, NLRP3 activation and iNOS expression level, compared with treated with them alone (Fig. 10D–F). MAPK signaling are widely recognized to modulate the expression of NLRP3 inflammasome pathway proteins and their downstream IL-1β as part of the inflammatory response, which can induce neuro-inflammation through the NF-κB and JNK pathways.[27] In our results, the inhibition of MAPK *via* specific inhibitor was down-regulated proinflammatory marker NO and its upstream regulator iNOS and significantly enhanced the effect of compound **7** on restraining inflammation through limiting the activation of the NLRP3 inflammasome. In summary, these findings demonstrated that compound **7** modulates inflammation *via* the MAPK/NLRP3 signaling pathway.

Conclusions

In summary, phytochemical investigation on agarwood chips from *A. malaccensis* led to the isolation of seven new compounds **1–7**, along with eleven previously identified compounds. The precise structures of these undescribed compounds were elucidated using extensive NMR data. The absolute configurations of **1–6** were determined by experimental ECD spectral analysis in comparison with the calculated ECD spectra data, whereas the absolute configuration of **7** was assigned by single-crystal X-ray crystallographic analysis. Isodaucane-type sesquiterpenoid skeleton (**3**) was first reported from genus *Aquilaria*. All isolated compounds did not show any cytotoxicity in the two-fold of test concentrations. *In vitro* assays of neuro-inflammatory targets from the agarwood of *A. malaccensis* showed that compounds **1–7** intensively inhibited NO production in LPS-treated BV2 microglial cells. Investigation of the expression and secretion of TNF-α, a key proinflammatory factor showed that compounds **2** and **7** significantly decreased levels after treatment with LPS in dose-dependent manner. The suppression of enzymatic activations of iNOS and COX-2 were investigated to demonstrate the pharmacological activity of against LPS-induced neuro-inflammatory responses by western blot analysis. The results showed that compounds **1–7** significantly reduced the expression of iNOS and then decreased NO production, whereas only compounds **2** and **7** were the most effective by significantly reducing COX-2 expression in a dose-dependent manner. In the mechanistic study, compound **7** regulated the LPS-induced neuro-inflammatory response by down-regulating the STAT1/AKT/MAPK pathway and modulates inflammation *via* the MAPK/NLRP3 signaling pathway. Our findings revealed the potential beneficial effects of *A. malaccensis* compounds in modulating microglial activation in the neuro-inflammatory treatment strategies, which further suggests the usage of this herbal medicine in traditional medicine by the modern therapeutic evidence.

Experimental section

General experimental procedures

Melting points were determined using a Mitamura Riken melting point apparatus (Japan). The optical rotations were measured on a JASCO P-2000 polarimeter (Japan) at 20 °C. IR spectrum was obtained from JASCO FT/IR 4200 (Japan). The ultraviolet (UV) and ECD spectra were measured on a Chirascan plus (Applied Photophysics Ltd, UK). NMR spectra were recorded on JEOL 400 (JEOL, JNM-ECZ400 s, Japan), Bruker AVANCE 500 MHz, and Bruker ASCENE (800 MHz) FT-NMR spectrometer (Germany); NMR solvents were purchased from Sigma-Aldrich (USA). HR-ESIMS were measured on an Agilent 6350 Q-TOF mass spectrometer (Agilent, USA). The X-ray crystallographic data were carried out on an Agilent SuperNova CCD detector system with Cu-Kα radiation ($\lambda = 1.54184$ Å). LC analyses were

carried out using an Agilent 1260 infinity system (USA) with a Phenomenex Luna 100 RP-C18 (250 × 4.6 mm i.d., 5 μm) column equipped with autosampler, DAD, and column thermostat. Semi-preparative HPLC were performed using a Gilson 321 pump and Gilson UV/VIS-155 detector system (Gilson, Middleton, USA) with a Phenomenex Luna 100 RP-C18 (250 × 10 mm i.d., 5 μm) column, flowrate 2 mL min^{-1}. Column chromatography was performed using silica gel 60 (0.040–0.063 mm; Merck, Germany) and Sephadex LH-20 (Amersham Bioscience AB, Uppsala, Sweden) as stationary phase. TLC was carried out on silica gel 60 F_{254} plates (Merck, Germany). All solvents used for isolation were purchased from Duksan pure chemical Co. (Gyeonggido, Korea). Solvents for HPLC were provided by J. T. Baker (USA).

Reagents and antibodies

SB202190 (S706), dexamethasone (D2915), LPS (*Escherichia coli*, 0111:B4), dimethyl sulfoxide (DMSO), sulfanilamide, *N*-(1-naphthyl)ethylenediamine dihydrochloride, and sodium nitrite were bought from Sigma-Aldrich (St. Louis, MO, USA). All the primary antibodies including those against iNOS (#13120), COX-2 (#12282), dehydrogenase (GAPDH) (#2118), Akt (#4685), p-Akt (Ser473) (#4060), JNK (#4672), p-JNK (#4668), NLRP3 (#15101), cleaved caspase1 (#89332), IL-1β (#12703), p-STAT1 (#9167), STAT1 (#9172) as well as the anti-rabbit horseradish peroxidase (HRP)-linked IgG (#7074) antibodies were purchased from Cell Signaling Technology (Beverly, MA, USA).

Plant material and isolation methods

The plant materials and separation methods used for the isolation and identification of *A. malaccensis* compounds are described in detail in the ESI.†

(4*S*, 5*S*, 7*S*, 8*S*, 10*S*, 11*R*)-7α,10β-Dihydroxy-4αH,5αH,8βH,11βH-guaia-1(2)-en-12,8α-olide (1). Colorless oil, $[\alpha]_D^{20}$ −81.2 (*c* 0.1, MeOH); ECD (MeOH) λ_{max} (Δε); CD (Δε): 217 (−51.5); ^{1}H NMR (800 MHz, CD_3OD) and ^{13}C NMR (200 MHz, CD_3OD) data: see Tables 1 and 2; HRESI-MS *m*/*z* 249.1479 $[M + H]^+$ (calcd for $C_{15}H_{21}O_3$, 249.1485).

Chamaejasmone G (2). Colorless oil, $[\alpha]_D^{20}$ −98.0 (*c* 0.1, MeOH). UV (MeOH) (log ε): 237 (1.69); ECD (MeOH) λ_{max} (Δε): 229 (−12.3), 325 (−1.15); ^{1}H NMR (400 MHz, CD_3OD) and ^{13}C NMR (100 MHz, CD_3OD) data: see Tables 1 and 2; HRESI-MS *m*/*z* 293.1380 $[M + H]^+$ (calcd for $C_{16}H_{20}O_5$, 293.1384).

Isodaucanranol A (3). Colorless oil, $[\alpha]_D^{20}$ −73.0 (*c* 0.1, MeOH). ECD (MeOH) λ_{max} (Δε): 210 (−1.94), 250 (0.47); ^{1}H NMR (800 MHz, $CDCl_3$) and ^{13}C NMR (200 MHz, $CDCl_3$) data: see Tables 1 and 3; HRESI-MS *m*/*z* 253.1790 $[M + H]^+$, (calcd for $C_{15}H_{25}O_3$, 237.1798).

(4*S*,5*R*,7*S*)-7α-Hydroxy-9(10)-ene-8-oxoeremophilane (4). Colorless oil; $[\alpha]_D^{20}$ −69.0 (*c* 0.07, MeOH); UV (MeOH) λ_{max} (log ε): 242 (3.34), 300 (2.01); ECD (MeOH) λ_{max} (Δε): 240 (−53.2), 324 (6.99); ^{1}H NMR (500 MHz, $CDCl_3$) and ^{13}C NMR (125 MHz, $CDCl_3$) data: see Tables 1 and 2; HRESI-MS *m*/*z* 237.1839 $[M + H]^+$ (calcd for $C_{15}H_{25}O_2$, 237.1855).

(1*S*,4*S*,5*S*)-1-Hydroxy-4,10-dimethyl-hexahydro-azulen-8-one (5). Colorless oil, $[\alpha]_D^{20}$ +9.6 (*c* 0.2, MeOH); UV (MeOH) λ_{max} (log ε): 236 (2.79), 300 (2.80); ECD (MeOH) λ_{max} (Δε): 220 (18.1), 274 (−0.43), 320 (−5.86); ^{1}H NMR (800 MHz, $CDCl_3$) and ^{13}C NMR (200 MHz, $CDCl_3$) data: see Tables 1 and 2; HRESI-MS *m*/*z* 217.1180 $[M + Na]^+$ (calcd for $C_{12}H_{18}O_2Na$, 217.1204).

(1*S*,4*S*,5*S*)-1-Hydroxy-4,9-dimethyl-hexahydro-5*H*-inden-5-one (6). Colorless oil; $[\alpha]_D^{20}$ −33.8 (*c* 0.22, MeOH); UV (MeOH) λ_{max} (log ε): 235 (2.91), 299 (3.16); ECD (MeOH) λ_{max} (Δε): 215 (23.47), 244 (−20.99); ^{1}H NMR (800 MHz, $CDCl_3$) and ^{13}C NMR (200 MHz, $CDCl_3$) data: see Tables 1 and 2; HREIMS *m*/*z* 181.1222 $[M + H]^+$, (calcd for $C_{11}H_{17}O_2$, 181.1229).

2-Hydroxy-22,23,24,25,26,27-hexanorcucurbit-1,5,16-triene-3,11,20-trione (7). Colorless needles (MeOH); mp 216–218 °C; $[\alpha]_D^{20}$ −7.0 (*c* 0.12, MeOH); UV (MeOH) λ_{max} (log ε): 240 (2.69), 275 (2.68); ^{1}H NMR (800 MHz, $CDCl_3$) and ^{13}C NMR (200 MHz, $CDCl_3$) data: see Table 3; HRESI-MS *m*/*z* 383.2204 $[M + Na]^+$, (calcd for $C_{24}H_{31}O_4$, 383.2222).

X-ray crystallographic data analysis for 7

A suitable crystal was selected and measured on a SuperNova, Dual, Cu at zero, AtlasS2 diffractometer with Cu Kα radiation (χ = 1.54184 Å). The crystal was kept at suitable temperature (100 K) during data collection. Using Olex2,[28] the structure was solved with the ShelXT[29] structure solution program using Direct Methods and refined with the ShelXL[30] refinement package using least squares minimization. Crystallographic data for compound 7 have been deposited at the Cambridge Crystallographic Data Centre (7: CCDC 2033830).

Orthorhombic, $C_{25}H_{34}O_5$ (M = 414.52 g mol^{-1}); space group $P2_12_12_1$ (no. 19), a = 10.0589(2) Å, b = 14.2921(3) Å, c = 15.1181(3) Å, V = 2173.43(8) $Å^3$, Z = 4, T = 99.8(7) K, μ(CuKα) = 0.697 mm^{-1}, D_{calc} = 1.267 g cm^{-3}, 21 475 reflections measured ($8.514 \leq 2\Theta \leq 153.356$), 4530 unique ($R_{int}$ = 0.0390, R_{sigma} = 0.0242) which were used in all calculations. The final R_1 was 0.0369 ($I > 2\sigma(I)$) and wR_2 was 0.0987 (all data). Flack parameter = −0.01(8)

Computational analysis and ECD calculations

All of the conformers of 1–6 in this study were searched using the MacroModel (version 2023-3, Schrödinger LLC) module with 'Mixed torsional/Low-mode sampling' in the MMFF force field. The conformational search was implemented in the gas phase with 50 kJ mol^{-1} energy window limit and 10 000 maximum number of steps were set to explore the potential conformers. The Polak–Ribiere Conjugate Gradient (PRCG) method was utilized to minimize conformers with 10 000 iterations and a 0.001 kJ (mol Å)$^{-1}$ convergence threshold on the Root Mean Square (RMS) gradient. From that search, the proposed conformers were selected within 20 kJ mol^{-1} in the MMFF force field and they were all subjected to geometry optimization using Tmolex 2023 (BIOVIA) with the density functional theory settings at B3-LYP/6-31G(d,p)

The ECD calculations for the possible conformers were performed at an identical theoretical level and basis sets. The calculated ECD spectra were simulated and superimposing each transition, where σ is the bandwidth at height 1/e and ΔE_i and R_i are the excitation energy and rotatory strength for transition i, respectively. In this study, the value of σ_v was 0.2 eV. Boltzmann-

averaged based on the calculated Gibbs free energy of each conformer can be found in the ESI† and ECD visualization was performed on GraphPad Prism 8.0 (GraphPad Software, San Diego, CA, USA).

$$\Delta\varepsilon(E) = \frac{1}{2.297 \times 10^{-39}} \frac{1}{\sqrt{2\pi\sigma}} \sum_{i}^{A} \Delta E_i R_i e^{[-(E-\Delta E_i/2\sigma)]^2}$$

Cell culture experiment

The BV-2 mouse microglia cell line was obtained from the Prof. Lee Sung Jung's research team in College of Medicine, Seoul National University and was cultured in Dulbecco's modified Eagle medium (DMEM; Welgene, South Korea), medium added with 10% fetal bovine serum (FBS; Thermo Fisher Scientific Inc., Lafayette, CA, U.S.A.) and 1% penicillin (Lonza, MD, USA) at 37 °C under a humidified atmosphere containing 5% CO_2.

Cell viability assay. Cell viability was measured by a colorimetric assay for assessing cell metabolic activity with the protocol described previously. BV-2 microglial cells were pre-incubated in DMEM/F12 (Gibco) and were seeded (5×10^4 cells per well) for 24 h into 96-well plates. After pre-culture, the cells were treated for 12 h with various concentrations of compound (2.5, 5, 10, 20, 40, 80 to 160 μM) in the presence or absence of 100 ng mL^{-1} LPS. After incubation for 12 h, BV-2 cells were treated with 10 μl of EZ-Cytox reagent (Daeil Lab Co., Ltd, Seoul, Republic of Korea) in each well and incubated for 30 min at 37 °C. Then The absorbance of each reaction product was measured using a microplate reader (Multiskan SkyHigh Photometer, Thermo Fisher Scientific Inc., Lafayette, CA, U.S.A.) at the wavelength of 450 nm. The results are presented as a percentage of the MTT absorbance of the control cells.

Measurement of nitric oxide. Cells were grown in 6-well plates (5×10^5 cells per well) for 24 h, and after incubation to 24 h, the cells were pre-administrated 2.5, 5 and 10 μM concentration of sample for 1 h, and were then treated with 100 ng mL^{-1} LPS for 12 h. The medium was collected and centrifuged at 13 000 rpm for removal of dead cells. The supernatant medium was collected and mixed with an equal volume (50 μl) of Griess reagents (1% sulfanilamide and *N*-(1-naphthyl) ethylenediamine dihydrochloride in 2.5% H_3PO_4) for 10 min incubating under room temperature, and nitric oxide concentration was measured by sodium nitrite standard curve at 540 nm using a microplate reader.

Enzyme-link immunosorbent assay (ELISA). In culture medium, all of ELISA kits were performed according to the manufacturer's protocols, including Mouse TNF alpha (ab208348) and IL-1beta ELISA Kit (ab241673, Abcam plc. Cambridge, UK). The data collected from the ELISA, a quantitative analysis to identify the exact cytokine production in the cell supernatant.

Total protein isolation from BV-2 cells. Total protein was isolated according to a previous study.[31] Briefly, the cells were washed 2 times with ice-cold PBS, then collected and centrifuged at 13 000 rpm for 5 min to remove the dead cell. And after discarding the supernatant, the collected cells were lysed with PRO-PREP protein extraction buffer (iNtRON, Gyeonggi, Republic of Korea) supplemented with PIC set III (Sigma-Aldrich, St. Louis, MO, U.S.A.) for 20 min incubation under 4 °C. The lysates were centrifuged (13 000 rpm) for 20 min. The quantification of protein was conducted with BCA protein assay kit (Thermo Fisher Scientific Inc., Lafayette, CA, U.S.A). Western blot loading samples were prepared with lysate and an equal volume of 2× NuPAGE LDS sample buffer (Thermo Fisher Scientific, Inc., Lafayette, CA, U.S.A.) with 10% 2-mercaptoethanol and stored at −80 °C until assay.

Western blot analysis. The total protein samples (10 μg) were separated using sodium dodecyl sulfate polyacrylamide gel electrophoresis (SDS−PAGE) with 10% acrylamide/bis gels and electrotransferred to polyvinylidene difluoride membranes (Millipore, Burlington, MA, U.S.A). Then, the membranes were blocked with 1× double blocker in TBST (Tris Buffered saline Tween) and incubated overnight under 4 °C with specific primary antibodies (1:1000). After the membranes were washed with TBST, they were incubated with secondary HRP conjugated IgG (1:2000) at room temperature for 1 h and visualized using enhanced chemiluminescence (ECL) reagents (Thermo Fisher Scientific). Densitometry analysis of the bands was performed with the fusion solo system (Vilber, Paris, France). The bands were quantified the intensities of protein by TotalLab TL120 software (TotalLab, Newcastle, UK).

Statistical analysis. Data were expressed as mean ± SEM of each independent replication. For comparison of three or more replications, data were analyzed by *t* test or one-way analysis of variance (ANOVA) followed by *t* test. A value of $P < 0.05$ was considered statistically significant. Statistical tests were carried out using GraphPad Prism 8.0 (GraphPad Software, San Diego, CA, USA).

Author contributions

Chi Thanh Ma: conceptualization, data curation, formal analysis, investigation, methodology, validation, visualization, writing – original draft, writing – review & editing. Tianqi Huang: data curation, formal analysis, investigation, methodology, validation, writing – original draft. Jae Sik Yu: data curation, formal analysis, investigation, methodology, software, validation, writing – original draft, writing – review & editing. Tu Loan Ly: conceptualization, investigation, project administration, resources. Kim Long Vu Huynh: methodology, project administration, resources. Sung Won Kwon: investigation, resources, supervision. Jeong Hill Park: investigation, resources, supervision. Hyun Ok Yang: conceptualization, project administration, supervision, writing – review & editing.

Conflicts of interest

The authors declare that they have no known competing financial interests or personal relationships that could have appeared to influence the work reported in this paper.

Acknowledgements

This research was supported by the Rural Development Administration of Korea (PJ017031 & PJ017076) and by the Ministry of

Science, ICT, and Future Planning through the National Research Foundation of Korea (2019K1A3A1A05088041). This work was also supported by a grant of Vietnam National Foundation for Science and Technology Development (NAFOSTED) (grant number 108.05–2019.07).

References

1 H. S. Kwon and S. H. Koh, Neuroinflammation in neurodegenerative disorders: the roles of microglia and astrocytes, *Transl. Neurodegener.*, 2020, **9**, 42.
2 S. Mandrekar-Colucci and G. E. Landreth, Microglia and inflammation in Alzheimer's disease, *CNS Neurol. Disord.: Drug Targets*, 2010, **9**, 156–167.
3 C. S. Subhramanyam, C. Wang, Q. Hu and S. T. Dheen, Microglia-mediated neuroinflammation in neurodegenerative diseases, *Semin. Cell Dev. Biol.*, 2019, **94**, 112–120.
4 U. K. Hanisch, Microglia as a source and target of cytokines, *Glia*, 2002, **40**, 140–155.
5 M. B. Graeber, W. Li and M. L. Rodriguez, Role of microglia in CNS inflammation, *FEBS Lett.*, 2011, **585**, 3798–3805.
6 R. Fürst and I. Zündorf, Plant-derived anti-inflammatory compounds: hopes and disappointments regarding the translation of preclinical knowledge into clinical progress, *Mediat. Inflamm.*, 2014, **2014**, 146832.
7 Q. Zhao, L. Zhu, S. Wang, Y. Gao and F. Jin, Molecular mechanism of the anti-inflammatory effects of plant essential oils: A systematic review, *J. Ethnopharmacol.*, 2022, **301**, 115829.
8 L. Qin, X. Wu, M. L. Block, Y. Liu, G. R. Breese, J. S. Hong, D. J. Knapp and F. T. Crews, Systemic LPS causes chronic neuroinflammation and progressive neurodegeneration, *Glia*, 2007, **55**, 453–462.
9 N. Marliani, A review: *Aquilaria* species as potential of pharmacological, *OISAA Journal of Indonesia Emas*, 2021, **4**, 49–53.
10 M. A. Eissa, Y. Z. H. Y. Hashim, S. S. S. Abdul Azziz, H. M. Salleh, M. L. M. Isa, N. M. Abd Warif, F. Abdullah, E. Ramadan and D. M. El-Kersh, Phytochemical Constituents of *Aquilaria malaccensis* Leaf Extract and Their Anti-Inflammatory Activity against LPS/IFN-γ-Stimulated RAW 264.7 Cell Line, *ACS Omega*, 2022, **7**, 15637–15646.
11 L.-R. Qiao, L. Yang, J.-H. Zou, L. Li, H. Sun, Y.-K. Si, D. Zhang, X. Chen and J. Dai, Neolignans and sesquiterpenes from cell cultures of *Stellera chamaejasme*, *Planta Med.*, 2012, **78**, 711–719.
12 M. Ishihara, T. Tsuneya and K. Uneyama, Fragrant sesquiterpenes from agarwood, *Phytochemistry*, 1993, **33**, 1147–1155.
13 Y. Liu, J. Ma, Q. Zhao, C. Liao, L. Ding, L. Chen, F. Zhao and F. Qiu, Guaiane-type sesquiterpenes from *Curcuma phaeocaulis* and their inhibitory effects on nitric oxide production, *J. Nat. Prod.*, 2013, **76**, 1150–1156.
14 M. M. Rao, H. Meshulam and D. Lavie, The constituents of *Ecballium elaterium* L. Part XXIII. Cucurbitacins and hexanorcucurbitacins, *J. Chem. Soc., Perkin Trans.*, 1974, **1**, 2552–2556.
15 J. Yang and Y. Chen, Studies on the constituents of *Aquilaria sinensis* (Lour.) Gilg. I. Isolation and structure elucidation of two new sesquiterpenes, baimuxinic acid and baimuxinal, *Acta Pharm. Sin.*, 1983, **18**, 191–198.
16 Z.-Y. Cheng, Z.-L. Hou, J.-X. Ren, D.-D. Zhang, B. Lin, X.-X. Huang and S.-J. Song, Guaiane-type sesquiterpenoids from the roots of *Stellera chamaejasme* L. and their neuroprotective activities, *Phytochemistry*, 2021, **183**, 112628.
17 D. J. Brecknell and R. M. Carman, Callitrin, callitrisin, dihydrocallitrisin, columellarin and dihydrocolumellarin, new sesquiterpene lactones from the heartwood of *Callitris columellaris*, *Tetrahedron Lett.*, 1978, **19**, 73–76.
18 B. Alpertunga, S. Imre, H. J. Cowe, P. J. Cox and R. H. Thomson, A photo artefact from linderazulene, *Tetrahedron Lett.*, 1983, **24**, 4461–4462.
19 D. S. Hays, M. Scholl and G. C. Fu, Organotin Hydride-Catalyzed Conjugate Reduction of α, β-Unsaturated Ketones, *J. Org. Chem.*, 1996, **61**, 6751–6752.
20 B. Wu, J. G. Lee, C. J. Lim, S. D. Jia, S. W. Kwon, G. S. Hwang and J. H. Park, Sesquiterpenoids and 2-(2-Phenylethyl)-4H-chromen-4-one (=2-(2-Phenylethyl)-4H-1-benzopyran-4-one) derivatives from *Aquilaria malaccensis* Agarwood, *Helv. Chim. Acta*, 2012, **95**, 636–642.
21 G. S. Hamilton, J.-H. Li and J. P. Steiner, Method of using neurotrophic sulfonamide compounds, *US Pat.*, US005721256A, 1998.
22 C. Seger, S. Sturm, M. E. Mair, E. P. Ellmerer and H. Stuppner, ^{1}H and ^{13}C NMR signal assignment of cucurbitacin derivatives from *Citrullus colocynthis* (L.) Schrader and *Ecballium elaterium* L. (Cucurbitaceae), *Magn. Reson. Chem.*, 2005, **43**, 489–491.
23 N. Suganthy, K. P. Devi, S. F. Nabavi, N. Braidy and S. M. Nabavi, Bioactive effects of quercetin in the central nervous system: Focusing on the mechanisms of actions, *Biomed. Pharmacother.*, 2016, **84**, 892–908.
24 J. Liu, H. Li, T. Gong, W. Chen, S. Mao, Y. Kong, J. Yu and J. Sun, Anti-neuroinflammatory Effect of Short-Chain Fatty Acid Acetate against Alzheimer's Disease via Upregulating GPR41 and Inhibiting ERK/JNK/NF-κB, *J. Agric. Food Chem.*, 2020, **68**, 7152–7161.
25 C. Ju Hwang, D.-Y. Choi, H. M. Park and T. J. Hong, NF-kB as a Key Mediator of Brain Inflammation in Alzheimer's Disease, *CNS Neurol. Disord.: Drug Targets*, 2019, **18**, 3–10.
26 T. K. Motawi, S. A. El-Maraghy, A. S. Kamel, S. E. Said and M. A. Kortam, Modulation of p38 MAPK and Nrf2/HO-1/NLRP3 inflammasome signaling and pyroptosis outline the anti-neuroinflammatory and remyelinating characters of Clemastine in EAE rat model, *Biochem. Pharmacol.*, 2023, **209**, 115435.
27 T. Lawrence, The nuclear factor NF-kappaB pathway in inflammation, *Cold Spring Harbor Perspect. Biol.*, 2009, **1**, a001651.
28 O. V. Dolomanov, L. J. Bourhis, R. J. Gildea, J. A. K. Howard and H. Puschmann, OLEX2: a complete structure solution,

refinement and analysis program, *J. Appl. Crystallogr.*, 2009, **42**, 339–341.

29 G. Sheldrick, SHELXT - Integrated space-group and crystal-structure determination, *Acta Crystallogr., Sect. A*, 2015, **71**, 3–8.

30 G. Sheldrick, Crystal structure refinement with SHELXL, *Acta Crystallogr., Sect. A*, 2015, **71**, 3–8.

31 D. Zhao, M. Y. Gu, J. L. Xu, L. J. Zhang, S. Y. Ryu and H. O. Yang, Anti-neuroinflammatory effects of 12-dehydrogingerdione in LPS-activated microglia through inhibiting AKT/IKK/NF-κb pathway and activating Nrf-2/HO-1 pathway, *Biomol. Ther.*, 2019, **27**, 92–100.